

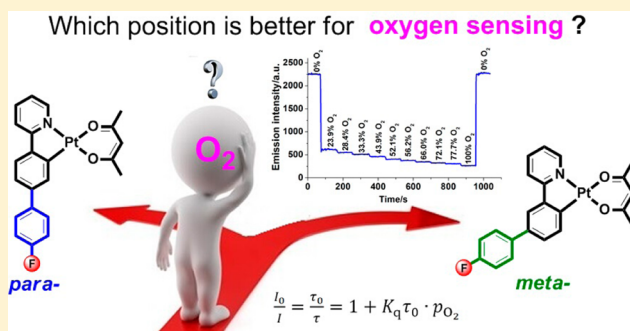
Photostable Fluorophenyl-Substituted Cyclometalated Platinum(II) Emitters for Monitoring of Molecular Oxygen in Real Time

Yang Xing, Chun Liu,* Jing-Hai Xiu, and Jiu-Yan Li

State Key Laboratory of Fine Chemicals, Dalian University of Technology, Linggong Road 2, Dalian 116024, China

Supporting Information

ABSTRACT: The effects of fluorophenyl substituents on the photoluminescence, redox properties, and oxygen sensing behaviors of the cyclometalated Pt(II) complexes are reported. The Pt(II) complexes with fluorophenyl substituents at the *para* position on the phenyl ring of 2-phenylpyridine (ppy) exhibit higher oxygen sensitivities than those at the *meta* position. Photodegradation tests demonstrate that the introduction of fluorophenyl substituents can strongly improve the photostability of cyclometalated Pt(II) complexes. Fast response and recovery times of oxygen sensing films are obtained in 3.0 s on going from 0% O₂ to 100% O₂ and in 4.0 s on going from 100% O₂ to 0% O₂ (95% recovery of the luminescence), respectively. The oxygen sensing films show excellent operational stability in 4000 s saturation O₂/N₂ cycles, which meets the requirement of monitoring molecular oxygen in real time.



INTRODUCTION

Determination of molecular oxygen is of great importance in various fields of science and technology.^{1–3} Compared with traditional analytical techniques, optical oxygen sensing can provide advantages of simple, quick, and nondestructive characteristics, low cost, small size, as well as low requirements for instrumental implementation. Optical oxygen sensing is based on the dynamic quenching process of the oxygen-sensitive probes (OSPs) by molecular oxygen, which is fully reversible and allows the determination of oxygen in real time.^{4–6} Among a variety of luminescent OSs, Pt(II) complexes are widely used due to their high photoluminescence quantum yields and significantly longer lifetimes.^{7,8} Pt(II) porphyrin complexes have often been reported as OSs in the literature.^{9–20} Only a few examples of cyclometalated Pt(II) complexes were tested in oxygen sensing.^{21–25}

To allow smooth oxygen diffusion and minimize probe self-quenching, OSs are usually doped into an oxygen permeable matrix. Typical matrices include ethyl cellulose,²⁶ poly(dimethylsiloxane),²⁷ and polystyrene.^{28,29} However, OSs immobilized in supporting matrices usually show a decrease of luminescence intensity (poor photostability) under continuous illumination. The reason comes from the photo-oxidation nature of OSs. Efforts have been made to heighten the photostability of OSs by modifying matrices¹⁹ and OSs.^{13–16,19,20} Notably, fluorinated matrices display large permeability of oxygen and stability against irradiation which is induced by the high electronegativity of fluorine. For example, Amao et al. reported that fluorinated polymers were excellent matrices for oxygen sensing.^{19,30–33} Fluorinated substituents can raise the oxidation potential and lower the electric density

of OSs. They also affect the π -conjugate of the intraligand and provide steric protection around the metal, which is a main consideration for increasing the quantum yield.^{34,35} Okura,²⁰ Amao,¹⁹ and Borisov^{13,14,16} have demonstrated that porphyrin ligands of Pt(II) complexes modified with fluorinated substituents could enhance the photostability. As far as we know, no efforts have been made to heighten the photostability of OSs by modification of the cyclometalated Pt(II) complexes with a fluorinated substituent. Very recently, we have successfully introduced a trifluoromethyl substituent ($-\text{CF}_3$) onto the cyclometalated Pt(II) complexes. And we found that the introduction of $-\text{CF}_3$ can effectively improve the photostability of the corresponding cyclometalated Pt(II) complexes and reduce photo-oxidation.³⁶

In this paper, we introduce bulky fluorophenyl substituents onto the cyclometalating ligand 2-phenylpyridine (ppy), such as a 3,4,5-trifluorophenyl substituent, to improve the photostability of corresponding cyclometalated Pt(II) complexes and to enhance the photoluminescence (PL) by preventing self-quenching and reducing photo-oxidation. In addition to that, we are interested in examining how the position of a fluorophenyl substituent affects the oxygen sensitivity of the Pt(II) complex from the viewpoint of optical oxygen sensing. Chemical structures of two series of the fluorophenyl-substituted cyclometalated Pt(II) complexes LXP1–LXP3 and LXM1–LXM3 are shown in Chart 1. These complexes possess 2-phenylpyridine with a fluorophenyl substituent at either the *para* or *meta* position of the phenyl ring.

Received: April 7, 2015

Chart 1. Structures of the Fluorophenyl-Substituted Pt(II) Complexes

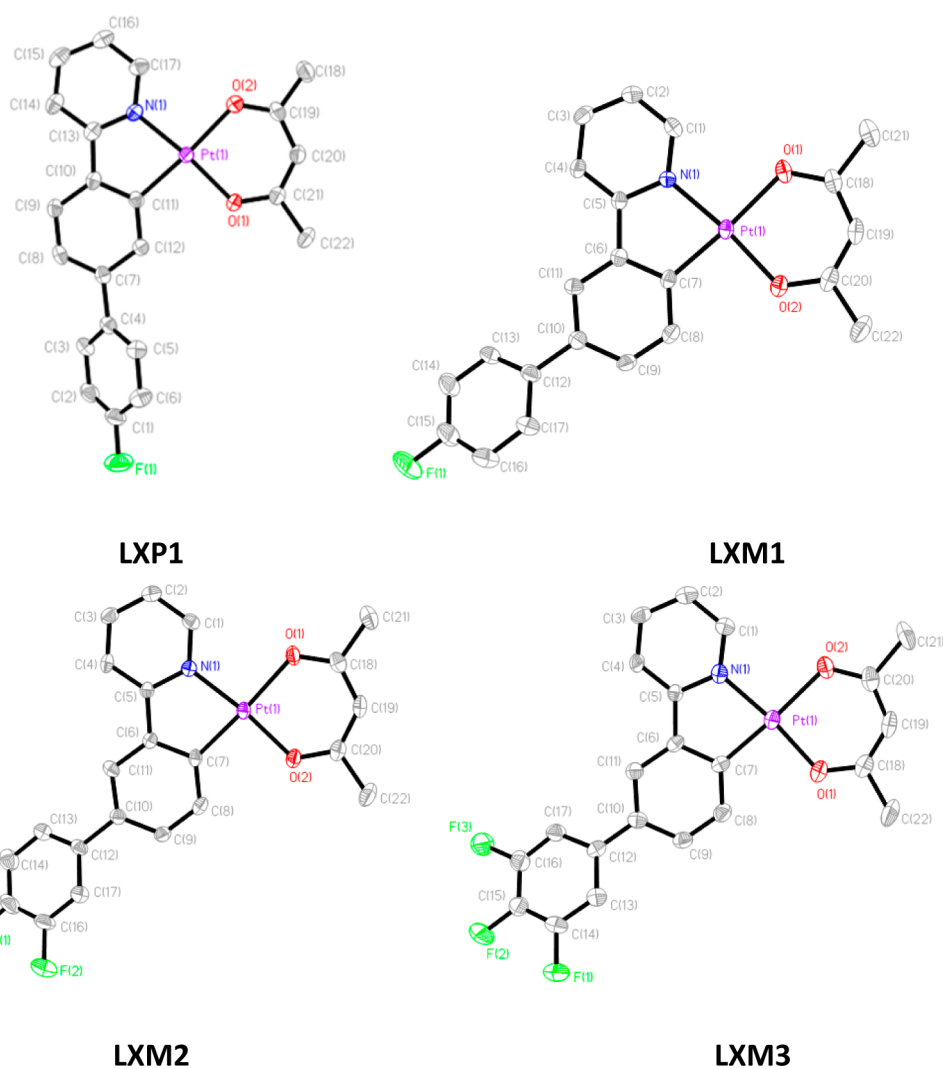
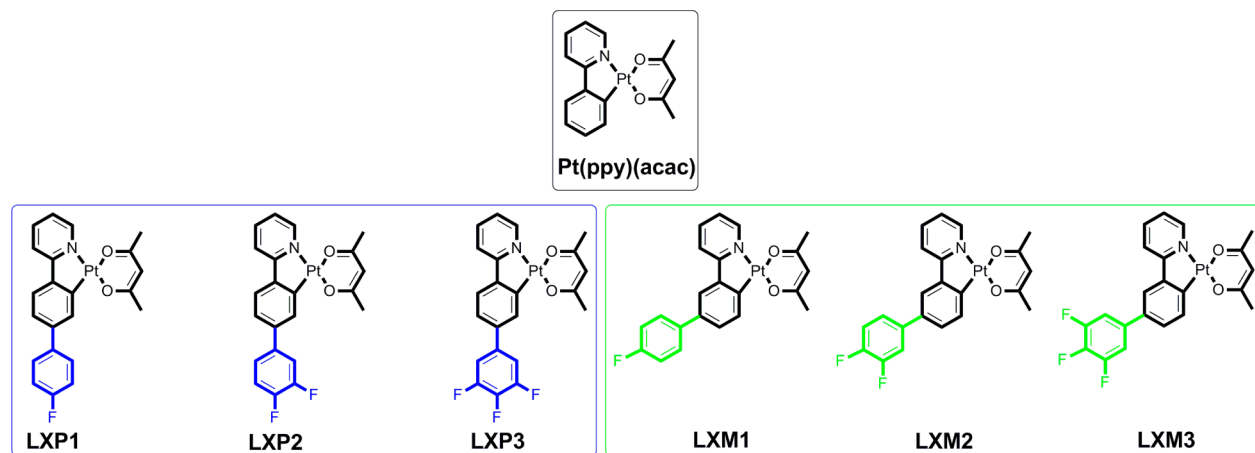


Figure 1. Perspective views of LXP1, LXM1, LXM2, and LXM3 (30% probability ellipsoids, hydrogen atoms are omitted for clarity).

RESULTS AND DISCUSSION

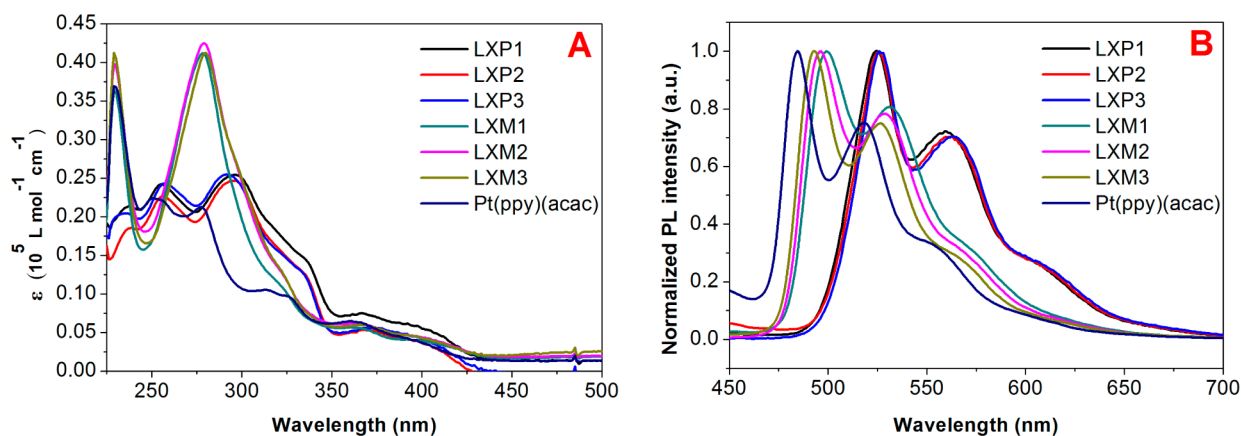
X-ray Structural Analysis. Single crystals suitable for X-ray diffraction analysis have been grown by slow diffusion of hexane into a chloroform solution of the complexes. Perspective views of LXP1, LXM1, LXM2, and LXM3 are shown in Figure 1. Key bonding parameters and selected crystallographic data are given

in Table 1 and Table S1 (see Supporting Information, SI). The Pt—N distances are in the range 1.984(5)–1.996(5) Å, which are slightly longer than those of common Pt—N bonds.^{37,38} The Pt—C distance is 1.944(7)–1.976(6) Å. The C—Pt—N and O—Pt—O angles are respectively 81.4(2)–81.9(2)° and 91.7(2)–92.1(2)°, which are similar to reported values (bond

Table 1. Selected Bond Length (Å) and Angles (deg) around the Metal Core in the Pt(II) Complexes

complexes	CCDC number	Pt—N	Pt—C	Pt—O ^a	C—Pt—N	O—Pt—O	Pt—Pt
LXP1	1038809	1.984(5)	1.976(6)	2.073(5) 1.994(4)	81.4(2)	91.7(2)	6.405(4)
LXM1	1000779	1.996(5)	1.964(6)	2.100(5) 1.997(5)	81.5(2)	91.8(2)	4.469(5)
LXM2	997714	1.988(4)	1.962(5)	2.103(3) 1.992(3)	81.9(2)	91.7(2)	4.473(6)
LXM3	1038810	1.994(6)	1.944(7)	2.109(5) 1.999(5)	81.9(2)	92.1(2)	4.466(5)

^aThe bond lengths in bold style are the Pt—O distances, where the O atoms of the acetylacetonate are trans to the C atoms of the fluorophenyl-substituted 2-phenylpyridine.

**Figure 2.** [A] Absorption spectra and [B] Emission (PL) spectra of all the Pt(II) complexes. 10^{-5} mol L⁻¹ in degassed CH₂Cl₂, 25 °C.**Table 2.** Photophysical and Electrochemical Data of All Pt(II) Complexes

complexes	absorption λ_{abs} (nm) ^a	emission λ_{em} (nm) ^b	Φ_{p} ^c	τ_{r} (μs) ^d	ΔT (°C) ^e
LXP1	237 (2.13), 255 (2.41), 296 (2.54), 334 (1.47), 366 (0.74), 405 (0.52)	525 , 559	0.18	4.11	276
LXP2	238 (1.85), 257 (2.26), 295 (2.46), 334 (1.28), 367 (0.53), 405 (0.33)	526 , 563	0.15	2.45	258
LXP3	235 (2.04), 257 (2.43), 291 (2.54), 333 (1.29), 374 (0.56), 405 (0.38)	526 , 565	0.22	1.39	271
LXM1	229 (3.63), 278 (4.12), 365 (0.56), 397 (0.40)	499 , 531	0.14	2.23	272
LXM2	229 (3.99), 279 (4.25), 361 (0.62), 397 (0.45)	496 , 528	0.22	1.74	278
LXM3	229 (4.12), 280 (4.12), 366 (0.60), 404 (0.41)	492 , 526	0.20	1.03	282
Pt(ppy)(acac)	229 (3.69), 250 (2.24), 277 (2.12), 314 (1.05), 365 (0.63), 389 (0.43)	486 , 518	0.15 ^f	2.60 ^f	294 ^g

^aMeasured in CH₂Cl₂ at a concentration of 10^{-5} M and extinction coefficients (10^4 M⁻¹ cm⁻¹) are shown in parentheses. ^bThe emission maxima ($\lambda_{\text{em}}^{\text{max}}$) are the values in bold style. ^cIn degassed CH₂Cl₂ relative to [Ir(ppy)₃acac] ($\Phi_{\text{p}} = 0.34$), ($\lambda_{\text{ex}} = 400$ nm). ^dMeasured in degassed CH₂Cl₂ at a sample concentration of ca. 10^{-5} M and the excitation wavelength was set at 425 nm for all the samples at 25 °C. ^e ΔT is the weight-reduction temperature. ^fRef 39. ^gRef 38.

lengths and angles around the metal core in 7-F, 7-H, 7-Me, 7-OMe, 9, and 11 in ref 38). The bond distances of the Pt—O edge trans to C atom 2.073(5)–2.109(5) Å are longer compared to those of the other Pt—O bonds 1.992(3)–1.999(5) Å, due to the strong trans influence from the C atom trans to O atom. The Pt—Pt distances are beyond the range of 2.7–3.5 Å. Thus, Pt—Pt interaction is impossible in the crystal. All other bond lengths around the Pt core are typical for cyclometalates and β -diketonate derivatives of Pt(II).³⁹

UV–Visible Absorption Spectra and Emission Spectra.

UV–visible absorption spectra of LXP1–LXP3 have similar band positions (Figure 2A and Table 2). They display strong bands up to 300 nm belong to intraligand (π – π^*) transitions. Lower energy absorption bands at 360 nm attributed to singlet and triplet metal-to-ligand charge transfer (¹MLCT and ³MLCT) transitions with spin-forbidden. The strong ligand field of the cyclometalating ligand shifts the d–d transitions to

high energy, putting them under the more intense ligand-centered (LC) transitions. Bands around 238 nm have similar intensity (about 20 000 M⁻¹ cm⁻¹) for LXP1–LXP3, while Pt(ppy)(acac) is stronger (37 000 M⁻¹ cm⁻¹). It is therefore attributed to a π – π^* transition involving the intraligand. UV–visible absorption spectra of LXM1–LXM3 exhibit three major absorption bands (Figure 2A and Table 2). The absorption bands at 238 nm and at 250–300 nm ($33\,000$ – $43\,000$ M⁻¹ cm⁻¹) are due to the spin-allowed singlet transitions of the intraligands. The singlet and triplet metal-to-ligand charge transfer (¹MLCT and ³MLCT) absorption bands appear at >370 nm ($\epsilon < 10\,000$ M⁻¹ cm⁻¹), with a peak position depended strongly on the identity of intraligand.

Fluorophenyl substituents at 2-phenylpyridine have significant influences on the emission properties of the complexes. We found that the emission maxima shifts to a longer wavelength when introducing fluorophenyl substituents at

either the *para* (p-) (LXP1–LXP3) or *meta* (m-) (LXM1–LXM3) position (Figure 2B and Table 2). The emission maxima for LXP1–LXP3, LXM1–LXM3, and Pt(ppy)(acac) are in region from 486 to 526 nm. The emission maxima are red-shifted about 40 nm for LXP1 (525 nm), LXP2 (526 nm), and LXP3 (526 nm) compared to the model emitter Pt(ppy)(acac) (486 nm). The emission maxima are red-shifted for LXM1 (499 nm), LXM2 (496 nm), and LXM3 (492 nm). The photoluminescence quantum yields Φ_p of all complexes range from 0.14 to 0.22 (Table 2).

Phosphorescence Lifetimes. The fluorophenyl substituents also have significant influence on phosphorescence lifetimes (Table 2). The lifetimes of Pt(II) complexes range from 1.03 to 4.11 μ s. These lifetimes in the microsecond regime suggest that triplet excited states contribute to light emission; that is, the complexes emit phosphorescence. The lifetimes decrease in the following order: LXP1 > LXM1; LXP2 > LXM2; LXP3 > LXM3. The phosphorescence lifetime of LXP1 (4.11 μ s) become longer compared to Pt(ppy)(acac) (2.60 μ s)³⁹ when the 4-fluorophenyl group is at the *para* position on the phenyl ring of 2-phenylpyridine. This result is useful information for designing novel Pt(II) complexes with a long lifetime. With the increase of fluorine atom on the fluorophenyl substituent, however, phosphorescence lifetimes are diminishing.

Electrochemical and Electronic Characterization. LXP1–LXP3 and LXM1–LXM3 show irreversible oxidation waves in the region of 0.65–0.71 V (Table 3 and SI Figure S1).

Table 3. Frontier Orbital Energy Levels of All Pt(II) Complexes

complexes	E_{ox} (V) ^a	HOMO (eV) ^b	LUMO (eV) ^c	E_g (eV) ^d
LXP1	0.65	−5.05	−2.57	2.48
LXP2	0.66	−5.06	−2.58	2.48
LXP3	0.70	−5.10	−2.64	2.46
LXM1	0.66	−5.06	−2.49	2.57
LXM2	0.67	−5.07	−2.48	2.59
LXM3	0.71	−5.11	−2.51	2.60
Pt(ppy)(acac)	0.53	−4.93	−2.25	2.68

^a0.1 M [Bu₄N]PF₆ in CH₂Cl₂, scan rate 100 mV s^{−1}, measured using saturated calomel electrode (SCE) as the standard. ^b E_{HOMO} (eV) = $-e(4.4 + E_{ox})$. ^c $E_{LUMO} = E_{HOMO} + E_g$. ^dEstimated from the absorption edge (λ_{edge}) of solid films by equation of $E_g = 1240/\lambda_{edge}$.

Compared to the oxidation potential (E_{ox}) of Pt(ppy)(acac) (0.53 V), E_{ox} for LXP1–LXP3 at 0.65 V, 0.66 V, 0.70 V, and for LXM1–LXM3 at 0.66 V, 0.67 V, 0.71 V, show that the introduction of a fluorophenyl substituent leads to effective raise of E_{ox} . The same result has been observed when introducing a trifluoromethyl substituent (−CF₃) on cyclometalated Pt(II) complexes.³⁶

Density Functional Theory (DFT) Calculations. The DFT calculations in Figure 3 show that the HOMOs of LXP1–LXP3 mainly consist of the platinum center, the phenyl ring of 2-phenylpyridine and acetyl acetone moiety, while the LUMOs are on the rings of cyclometalating ligands. The HOMOs of LXM1–LXM3 mainly consist of the platinum center, biphenyl group of cyclometalating ligands and acetyl acetone moiety. The LUMOs are on the 2-phenylpyridine and the platinum center. The increase of strong electron-withdrawing group (−F) lower the energy level of LUMO and HOMO obviously by increasing the electron affinity of the C[^]N ligand. These

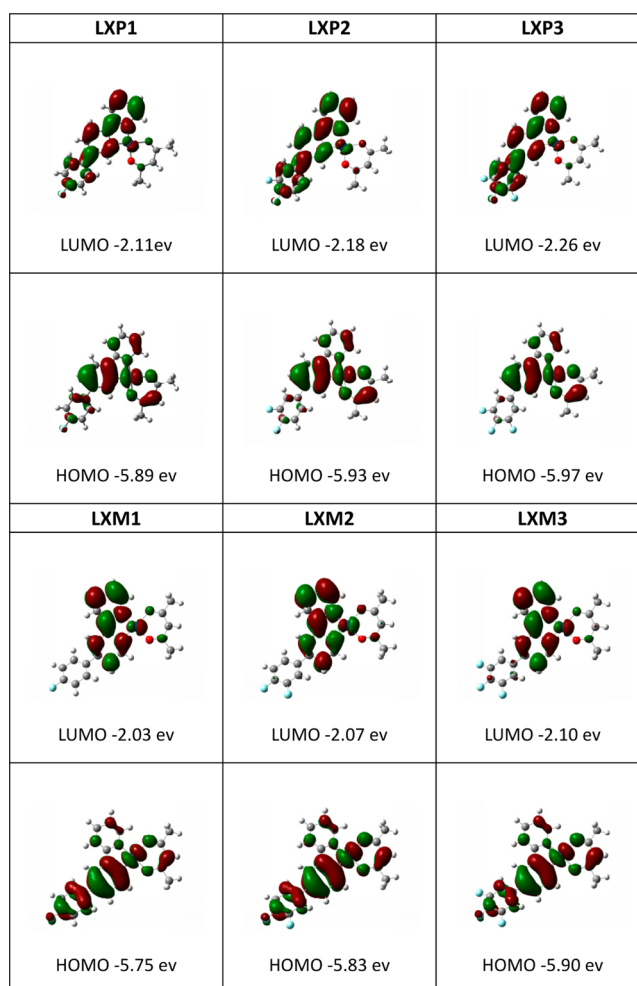


Figure 3. Kohn–Sham HOMO and LUMO for LXP1–LXP3 and LXM1–LXM3 for the ground state geometry at the DFT/M06/PCM = CH₂Cl₂ level of theory.

calculated energy levels in Figure 3 and Table 3 should not be overinterpreted, because the appropriate difference between experimental values and calculated values is acceptable.⁴⁰

Fitting Formula of Oxygen Sensing. Optical oxygen sensors depend on the diffusion-controlled quenching of OSPs by oxygen. Diffusion-controlled quenching is reflected by Stern–Volmer eq 1. K_q is the quenching rate constant, and p_{O_2} is the partial pressure of oxygen. I is the phosphorescence intensity, and τ is the lifetime of an OSP. I_0 and τ_0 are the corresponding values in the absence of oxygen.

$$\frac{I_0}{I} = \frac{\tau_0}{\tau} = 1 + K_q \tau_0 p_{O_2} \quad (1)$$

For heterogeneous oxygen sensing, a two-site model⁴¹ eq 2 was required to fit the Stern–Volmer plots. There exist two portions which are defined as f_1 and f_2 ($f_1 + f_2 = 1$). K_{SV1} and K_{SV2} are the quenching rate constants for two portions.

$$\frac{I_0}{I} = \frac{\tau}{\tau_0} = \frac{f_1}{1 + K_{SV1} p_{O_2}} + \frac{f_2}{1 + K_{SV2} p_{O_2}} \quad (2)$$

Parameter weighted quenching constant K_{SV}^{app} ($K_{SV}^{app} = f_1 \times K_{SV1} + f_2 \times K_{SV2}$) is the guide of the sensitivity of an oxygen sensor.

Photostability of Oxygen Sensing Films. The photostability of OSPs is of great importance for the detection of oxygen concentrations under continuous irradiation. Hartmann and co-workers reported the experimental method for photodegradation.⁴² In this work, the weight content of all Pt(II) complexes immobilized in an ethyl cellulose (EC) film is 0.5 wt %. And the film thickness is about 5.88 μm . Photostability of oxygen sensing films immobilized with Pt(II) complexes were estimated upon continuous irradiation with a 254 nm 16 W UV lamp under air atmosphere. The power density on the films is 23.4 W/m^2 . After irradiation, the PL measurements performed under N_2 atmosphere. Data presented in Figure 4 indicate that

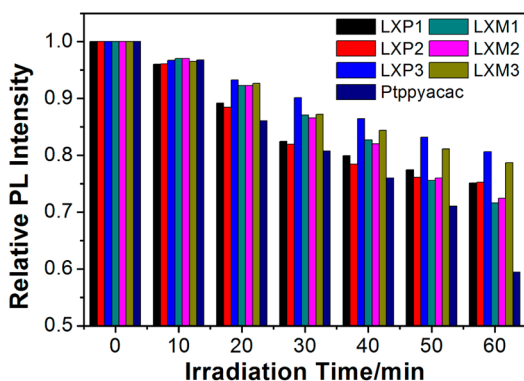


Figure 4. Photodegradation histograms of oxygen sensing films immobilized with Pt(II) complexes. The power density on the films is 23.4 W/m^2 .

photostability of fluorophenyl substituted Pt(II) complexes (LXP1–LXP3 and LXM1–LXM3) is much higher than that of Pt(ppy)(acac) after 60 min irradiation. In fact, decreases in intensity of LXP1–LXP3 by 24.9%, 24.8%, and 19.4% are observed compared to Pt(ppy)(acac) by 41%. While decreases in intensity of LXM1–LXM3 by 28.4%, 27.6%, and 21.2% are observed after 60 min irradiation. With the increase of the fluorine atom at the fluorophenyl substituent, Pt(II) complexes demonstrate higher photostability.

In general, the photo-oxidation reactivity of the Pt(II) complexes is determined by its excited-state oxidation potential.⁴³ The zero-zero emission energy (E_{00}), the ground-state oxidation potential (E_{ox}), and the excited-state oxidation potential (E_{ox}^*) of a Pt(II) complex can be estimated from eq 3:⁴⁴

$$E_{\text{ox}}^* = E_{\text{ox}} - E_{00} \quad (3)$$

Using the emission maxima ($\lambda_{\text{em}}^{\text{max}}$) of the Pt(II) complexes as calculation of E_{00} together with the E_{ox} in Table 3, the E_{ox}^* was calculated (Table 4). It is clear that the E_{ox}^* of Pt(II) complexes are in the sequence of LXP3 > LXP2 > LXP1 > Pt(ppy)(acac); LXM3 > LXM2 = LXM1 > Pt(ppy)(acac). Notably, for the Pt(II) complexes with same number of fluorine atom, *para*-fluorophenyl substituents on the phenyl ring cause a greater anodic shift of E_{ox}^* than *meta*-fluorophenyl substituents (LXP1 > LXM1; LXP2 > LXM2; LXP3 > LXM3). The order is consistent with the photostability order of the Pt(II) complexes in photodegradation test (Figure 4). Although there are errors in the E_{00} values caused by the calculation method, the errors did not affect the order of E_{ox}^* . Hence the inductive effect of the fluorophenyl substituents raises the excited-state oxidation potentials of the Pt(II) complexes, which makes the molecules

Table 4. Oxidation Potentials for All the Pt(II) Complexes

complexes	E_{00} (V) ^a	E_{ox} (V) ^b	E_{ox}^* (V) ^c
LXP1	2.36	0.65	−1.71
LXP2	2.35	0.66	−1.69
LXP3	2.35	0.70	−1.65
LXM1	2.49	0.66	−1.83
LXM2	2.50	0.67	−1.83
LXM3	2.52	0.71	−1.81
Pt(ppy)(acac)	2.55	0.53	−2.02

^a $E_{00} = 1240/\lambda_{\text{em}}^{\text{max}}$; ^b0.1 M [Bu₄N]PF₆ in CH₂Cl₂, scan rate 100 mV s^{−1}, measured using saturated calomel electrode (SCE) as the standard. ^c $E_{\text{ox}}^* = E_{\text{ox}} - E_{00}$.

less reactive to photo-oxidation processes and increases its photostability.

Time-Dependent Response of Oxygen Sensing Films.

The dynamic responses of oxygen sensing films were investigated against small steps of O₂ concentration variation (Figure 5). The oxygen sensing films in N₂ exhibit intense emission. All the films are sensitive to oxygen with the phosphorescence intensity changing stepwise and reversibly to different O₂ concentrations. The oxygen sensing data were fitted by the two-site model (Figure 6) and weighted quenching constant $K_{\text{q}}^{\text{app}}$ are summarized in SI Table S2. All of the large quenchable components (f_1) > 91% show the wide liner range. The oxygen sensing film of LXP1 ($K_{\text{q}}^{\text{app}} = 0.0203 \text{ Torr}^{-1}$) provides outstanding oxygen sensitivity. The fluorophenyl substituent at either the *para* or *meta* position on the phenyl ring of 2-phenylpyridine could reduce the intermolecular interaction of the complexes and prevent self-quenching compared to Pt(ppy)(acac), resulting in increased oxygen sensitivities. Overall, the oxygen sensitivities are in the following order: LXP1 > LXM1; LXP2 > LXM2; LXP3 > LXM3. The fluorophenyl group at *para* position on the phenyl ring of 2-phenylpyridine (LXP1–LXP3) demonstrated higher oxygen sensitivities than *meta* position (LXM1–LXM3). The oxygen sensitivities are consistent with their triplet lifetimes.

Operational Stability of Oxygen Sensing Films.

Figure 7 shows an operational stability test conducted by luminescence intensity of oxygen sensing film of LXP3. The I_0 and I_{100} of an oxygen sensing film is constant, and the quenching and recovering cycles are fully reversible, which exhibits excellent operational stability in 12 cycles when N₂ and O₂ are switched in 4000 s. Very fast response time of LXP3 immobilized in EC was obtained at 3.0 s on going from 0% O₂ to 100% O₂ and recovery time at 4.0 s (95% recovery of the luminescence) on going from 100% O₂ to 0% O₂, which can meet the requirement of monitoring molecular oxygen in real time.

CONCLUSIONS

In summary, six new fluorophenyl-substituted Pt(II) complexes (LXP1–LXP3 and LXM1–LXM3) have been synthesized and characterized by means of spectroscopic and electrochemical methods and X-ray crystal structure. All Pt(II) complexes exhibit intense phosphorescence emissions at room temperature. By changing the position of fluorophenyl substituents, the emission maxima were tuned in the wavelength region from 492 to 526 nm. The oxygen sensitivity of Pt(II) complexes was evaluated according to the Stern–Volmer equation. The fluorophenyl substituents at the *para* position on the phenyl ring of ppy provided higher oxygen sensitivities than those at the *meta* position. Fast response time at 3.0 s on going from 0%

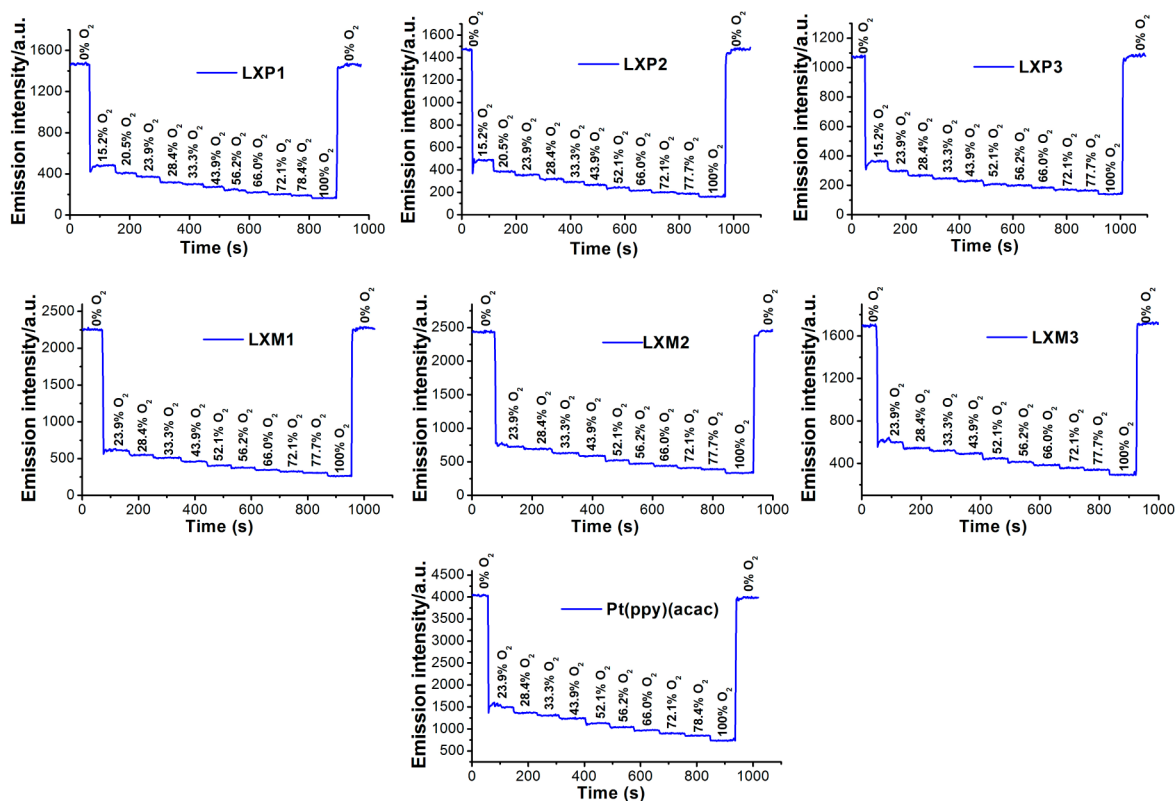


Figure 5. Time-dependent emission intensity response of oxygen sensing films of all the Pt(II) complexes immobilized in EC under stepwise change O_2 concentrations, 25 °C, slit width_{ex/em} = 2.5/2.5 nm.

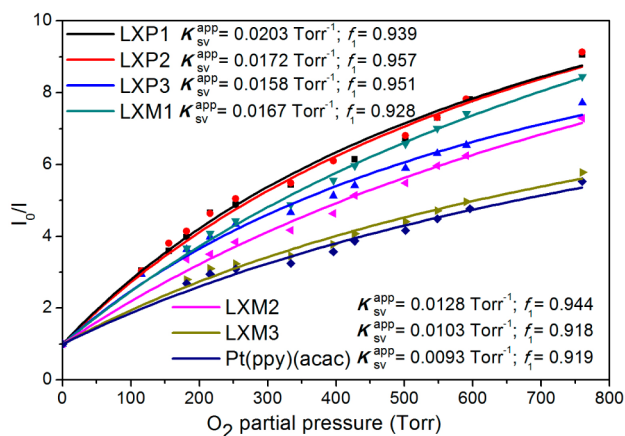


Figure 6. Stern–Volmer plots for the oxygen sensing films of all the Pt(II) complexes immobilized in EC. Intensity ratios I_0/I versus O_2 partial pressure.

O_2 to 100% O_2 and recovery time at 4.0 s on going from 100% O_2 to 0% O_2 (95% recovery of the luminescence) were observed. Importantly, the introduction of a fluorophenyl substituent can strongly improve the photostability of cyclometalated Pt(II) complexes to reduce photo-oxidation. These results are important information for designing novel photostable OSPs for monitoring of molecular oxygen in real time.

EXPERIMENTAL SECTION

Materials and Methods. Unless otherwise noted, all of the cross-coupling reactions for preparing the ligands were carried out in air. 2-Bromopyridine was purchased from Alfa Aesar. Fluorophenyl boronic acids were purchased from Trusyn Chem-Tech Co., Ltd., China. Other

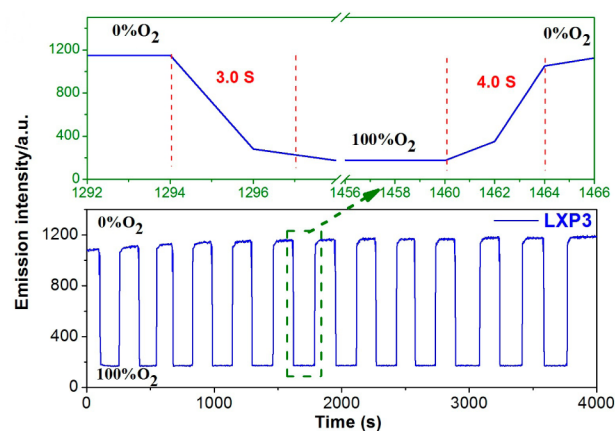


Figure 7. Time trace curve of LXP3 immobilized in EC to O_2/N_2 saturation cycles, 25 °C, slit width_{ex/em} = 2.5/2.5 nm.

chemicals were purchased from commercial sources and used without further purification. 1H NMR and ^{13}C NMR spectra were recorded on a 400 MHz Varian Unity Inova spectrophotometer. Mass spectra were recorded with a MALDI micro MX spectrometer. Phosphorescence lifetimes were determined on a steady and transient state fluorometer (FLS920, Edinburgh Analytical Instruments Ltd.). Thermogravimetric analysis (TGA) was performed on a TGA Q500 instruments. The Pt(II) complexes were stored at 30 °C for 10 min, then heated at a heating rate of 10 °C/min under nitrogen atmosphere. Absorption spectra were recorded by Lambda 750S UV/vis/NIR spectrometer (PerkinElmer). Emission spectra were recorded by HITACHI F-7000 fluorescence spectrophotometer. Cyclic voltammograms of all the Pt(II) complexes were recorded on an electrochemical workstation (BAS100B/W, USA) at room temperature.

Synthetic procedure of cyclometalated Pt(II) complexes LXP1–LXP3 and LXM1–LXM3: The cyclometalating ligand (0.20 mmol) was reacted with 1.2 equiv K_2PtCl_4 (0.24 mmol, 99.0 mg) in a mixture of 2-ethoxyethanol and water (6 mL/2 mL) at 100 °C for 16–24 h to afford a platinum dimer, which was subsequently reacted with 10 equiv of the chelating diketone (1 mmol, 102.5 μ L) and 10 equiv of Na_2CO_3 (1 mmol, 0.106 g) in 2-ethoxyethanol at 100 °C for 18–24 h.

LXP1: yellow solid; yield 70.0%. 1H NMR (400 MHz, $CDCl_3$): δ 9.01 (d, $J = 5.5$ Hz, 1H), 7.86–7.74 (m, 2H), 7.70–7.60 (m, 3H), 7.49 (d, $J = 8.1$ Hz, 1H), 7.28 (s, 1H), 7.13 (t, $J = 8.5$ Hz, 3H), 5.49 (s, 1H), 2.02 (s, 6H). ^{13}C NMR (101 MHz, $CDCl_3$): δ 185.8, 184.2, 167.9, 163.7, 161.2, 147.3, 143.8, 140.8, 139.2, 138.2, 128.9, 123.3, 122.6, 121.1, 118.4, 115.5, 115.3, 102.5, 28.2, 27.2. HRMS (ESI): $C_{22}H_{19}FNO_2Pt$. Calcd.: 543.1044 $[M + H]^+$. Found: 543.1043 $[M + H]^+$.

LXP2: yellow solid; yield 65.0%. 1H NMR (400 MHz, $CDCl_3$): δ 9.02 (dd, $J = 5.8, 0.8$ Hz, 1H), 7.82 (td, $J = 8.0, 1.5$ Hz, 1H), 7.76 (d, $J = 1.8$ Hz, 1H), 7.64 (d, $J = 7.8$ Hz, 1H), 7.53–7.44 (m, 2H), 7.44–7.35 (m, 1H), 7.22 (m, 2H), 7.13 (ddd, $J = 7.3, 5.9, 1.4$ Hz, 1H), 5.49 (s, 1H), 2.03 (d, $J = 3.6$ Hz, 6H). ^{13}C NMR (101 MHz, $CDCl_3$): δ 185.9, 184.3, 167.7, 147.4, 144.4, 139.6, 139.4, 138.9, 138.9, 138.2, 128.7, 123.3, 122.5, 121.3, 118.5, 117.3, 117.2, 116.2, 116.0, 102.6, 28.2, 27.2. HRMS (ESI): $C_{22}H_{18}F_2NO_2Pt$. Calcd.: 561.0953 $[M + H]^+$. Found: 561.0949 $[M + H]^+$.

LXP3: yellow solid; yield 73.1%. 1H NMR (400 MHz, $CDCl_3$): δ 9.03 (d, $J = 5.1$ Hz, 1H), 7.83 (td, $J = 8.0, 1.5$ Hz, 1H), 7.73 (d, $J = 1.9$ Hz, 1H), 7.64 (d, $J = 8.0$ Hz, 1H), 7.49 (d, $J = 8.0$ Hz, 1H), 7.29 (dd, $J = 9.0, 6.6$ Hz, 2H), 7.22 (dd, $J = 8.0, 1.9$ Hz, 1H), 7.15 (ddd, $J = 7.3, 5.9, 1.4$ Hz, 1H), 5.50 (s, 1H), 2.03 (d, $J = 5.9$ Hz, 6H). ^{13}C NMR (101 MHz, $CDCl_3$): δ 185.9, 184.3, 167.5, 150.1, 147.5, 145.0, 139.6, 138.6, 138.3, 137.9, 128.5, 123.4, 122.3, 121.5, 118.6, 111.2, 111.0, 102.6, 28.2, 27.2. HRMS (ESI): $C_{22}H_{17}F_3NO_2Pt$. Calcd.: 579.0856 $[M + H]^+$. Found: 579.0963 $[M + H]^+$.

LXM1: yellow solid; yield 73.2%. 1H NMR (400 MHz, $CDCl_3$): δ 9.03 (dd, $J = 5.8, 0.8$ Hz, 1H), 7.83 (td, $J = 8.0, 1.5$ Hz, 1H), 7.73–7.67 (m, 2H), 7.58 (td, $J = 5.3, 2.7$ Hz, 3H), 7.40 (dd, $J = 7.9, 1.9$ Hz, 1H), 7.17–7.09 (m, 3H), 5.49 (s, 1H), 2.02 (d, $J = 3.7$ Hz, 6H). ^{13}C NMR (101 MHz, $CDCl_3$): δ 185.8, 184.2, 168.0, 163.3, 160.9, 147.4, 145.2, 138.2, 137.9, 135.7, 131.1, 128.3, 121.5, 121.4, 118.4, 115.6, 115.4, 102.5, 28.3, 27.1. HRMS (EI): $C_{22}H_{18}FNO_2Pt$. Calcd.: 542.0969 $[M]^+$. Found: 542.0966 $[M]^+$.

LXM2: yellow solid; yield 55.5%. 1H NMR (400 MHz, $CDCl_3$): δ 9.04 (d, $J = 5.1$ Hz, 1H), 7.89–7.81 (m, 1H), 7.70 (dd, $J = 7.9, 3.2$ Hz, 2H), 7.56 (d, $J = 1.8$ Hz, 1H), 7.47–7.30 (m, 3H), 7.24–7.13 (m, 2H), 5.50 (s, 1H), 2.03 (d, $J = 3.3$ Hz, 6H). ^{13}C NMR (101 MHz, $CDCl_3$): δ 185.9, 184.2, 167.8, 147.5, 145.3, 139.0, 138.3, 134.6, 131.2, 127.9, 122.5, 122.4, 121.6, 121.4, 118.5, 117.5, 117.3, 115.6, 115.4, 102.6, 28.3, 27.1. HRMS (EI): $C_{22}H_{17}F_2NO_2Pt$. Calcd.: 560.0875 $[M]^+$. Found: 560.0884 $[M]^+$.

LXM3: yellow solid; yield 50.0%. 1H NMR (500 MHz, $CDCl_3$): δ 9.04 (d, $J = 5.6$ Hz, 1H), 7.85 (dd, $J = 11.3, 4.2$ Hz, 1H), 7.70 (d, $J = 7.9$ Hz, 2H), 7.53 (d, $J = 1.5$ Hz, 1H), 7.34 (dd, $J = 7.9, 1.7$ Hz, 1H), 7.22 (dd, $J = 8.7, 6.6$ Hz, 2H), 7.17 (t, $J = 6.2$ Hz, 1H), 5.50 (s, 1H), 2.03 (d, $J = 3.8$ Hz, 6H). ^{13}C NMR (101 MHz, $CDCl_3$): δ 185.9, 184.3, 167.6, 152.7, 150.2, 147.5, 145.5, 140.0, 138.4, 133.6, 131.3, 127.6, 121.7, 121.1, 118.5, 110.5, 110.3, 102.6, 28.2, 27.1. HRMS (EI): $C_{22}H_{16}F_3NO_2Pt$. Calcd.: 578.0781 $[M]^+$. Found: 578.0787 $[M]^+$.

Density Functional Theory (DFT) Calculations. The structures of the complexes were optimized using density functional theory (DFT) with the B3LYP functional and 6-31G(d)/LanL2DZ basis set.^{23–25} Calculations have been carried out considering solvent effects (CH_2Cl_2) with the polarizable continuum model (PCM).^{45,46} The 6-31G(d) basis set was employed for C, H, N, O, and the LanL2DZ basis set was used for Pt(II). All these calculations were performed with the Gaussian 09 software package.⁴⁷

Electrochemical and Electronic Characterization. The electrochemical properties of all the Pt(II) complexes were examined using cyclic voltammetry. Using Bu_4NPF_6 (0.1 mol) as the supporting electrolyte; values are obtained at a scan rate of 100 $mV s^{-1}$ using saturated calomel electrode (SCE) as the standard.⁴⁸

Oxygen Sensing. General procedure of oxygen sensing film on 0.5% weight percents: EC (9.95 mg) was dissolved in CH_2Cl_2 (0.90 mL) and then 0.10 mL LXP1 (0.5 mg/mL) in CH_2Cl_2 was added to the solution. After thoroughly mixing, the solution (0.10 mL) was coated on a transparent quartz plate ($r = 7.0$ mm) and slowly evaporated at room temperature. The film was dried for 24 h to remove the potential cocrystallized solvent molecules before oxygen sensing experiments. Then a yellow transparent EC oxygen sensing film was obtained. The thickness of the film is about 5.88 μm .

The specific concentrations of oxygen in nitrogen at atmospheric pressure (from 0–100% in volume fraction) were generated with two tube flowmeter (Figure 8A). The transparent quartz plate (Figure 8B)

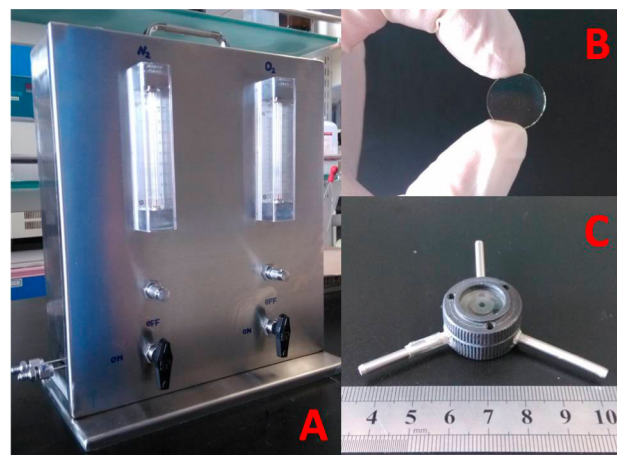


Figure 8. (A) N_2 and O_2 tube flowmeters. (B) The transparent quartz plate whose inner surface is covered with oxygen sensing film. (C) The home-assembled sealed flow cell in which transparent quartz plate is placed.

coated with oxygen sensing film was placed into our home-assembled sealed flow cell (Figure 8C). Dead volume of the flow cell is 0.1 mL. The time trace curves and dynamic emissive intensity response of all the Pt(II) oxygen sensing films were recorded by HITACHI F-7000 fluorescence spectrophotometer.³⁶

■ ASSOCIATED CONTENT

📄 Supporting Information

X-ray crystallographic data of LXP1, LXM1, LXM2, and LXM3 in CIF format. Detailed synthetic schemes and procedures; characterization data; and crystal data for LXP1, LXM1, LXM2, and LXM3. The Supporting Information is available free of charge on the ACS Publications website at DOI: 10.1021/acs.inorgchem.5b00775.

■ AUTHOR INFORMATION

Corresponding Author

*E-mail: cliu@dlut.edu.cn.

Notes

The authors declare no competing financial interest.

■ ACKNOWLEDGMENTS

The authors thank the financial support from the National Natural Science Foundation of China (21276043, 21421005).

■ REFERENCES

- (1) Semenza, G. L. *Science* **2007**, *318*, 62–64.
- (2) Sakadžić, S.; Roussakis, E.; Yaseen, M. A.; Mandeville, E. T.; Srinivasan, V. J.; Arai, K.; Ruvinskaya, S.; Devor, A.; Lo, E. H.; Vinogradov, S. A. *Nat. Methods* **2010**, *7*, 755–759.

- (3) Lehner, P.; Staudinger, C.; Borisov, S. M.; Klimant, I. *Nat. Commun.* **2014**, *5*, 4460 DOI: 10.1038/ncomms5460.
- (4) Wang, X. D.; Wolfbeis, O. S. *Chem. Soc. Rev.* **2014**, *43*, 3666–3761.
- (5) Marín-Suárez, M.; Curchod, B. F. E.; Tavernelli, I.; Rothlisberger, U.; Scopelliti, R.; Jung, I.; Di Censo, D.; Grätzel, M.; Fernández-Sánchez, J. F.; Fernández-Gutiérrez, A.; Nazeeruddin, M. K.; Baranoff, E. *Chem. Mater.* **2012**, *24*, 2330–2338.
- (6) Pulido, C.; Esteban, Ó. *Sens. Actuators, B* **2013**, *184*, 64–69.
- (7) Yeh, T.-S.; Chu, C.-S.; Lo, Y.-L. *Sens. Actuators, B* **2006**, *119*, 701–707.
- (8) Suzuki, S.; Sugimura, R.; Kozaki, M.; Keyaki, K.; Nozaki, K.; Ikeda, N.; Akiyama, K.; Okada, K. *J. Am. Chem. Soc.* **2009**, *131*, 10374–10375.
- (9) Zhao, Q.; Li, F.; Huang, C. *Chem. Soc. Rev.* **2010**, *39*, 3007–3030.
- (10) Xiang, H.; Zhou, L.; Feng, Y.; Cheng, J.; Wu, D.; Zhou, X. *Inorg. Chem.* **2012**, *51*, S208–S212.
- (11) Zhao, Q.; Zhou, X.; Cao, T.; Zhang, K. Y.; Yang, L.; Liu, S.; Liang, H.; Yang, H.; Li, F.; Huang, W. *Chem. Sci.* **2015**, *6*, 1825–1831.
- (12) Chu, C.-S.; Lo, Y.-L. *Sens. Actuators, B* **2007**, *124*, 376–382.
- (13) Borisov, S. M.; Nuss, G.; Klimant, I. *Anal. Chem.* **2008**, *80*, 9435–9442.
- (14) Borisov, S. M.; Nuss, G.; Haas, W.; Saf, R.; Schmuck, M.; Klimant, I. *J. Photochem. Photobiol., A* **2009**, *201*, 128–135.
- (15) Borisov, S. M.; Zenkl, G.; Klimant, I. *ACS Appl. Mater. Interfaces* **2010**, *2*, 366–374.
- (16) Borisov, S. M.; Lehner, P.; Klimant, I. *Anal. Chim. Acta* **2011**, *690*, 108–115.
- (17) Tian, Y.; Shumway, B. R.; Gao, W.; Youngbull, C.; Holl, M. R.; Johnson, R. H.; Meldrum, D. R. *Sens. Actuators, B* **2010**, *150*, 579–587.
- (18) Chu, C.-S.; Lo, Y.-L. *Sens. Actuators, B* **2011**, *155*, 53–57.
- (19) Amao, Y.; Miyashita, T.; Okura, I. *J. Fluorine Chem.* **2001**, *107*, 101–106.
- (20) Lee, S.-K.; Okura, I. *Anal. Commun.* **1997**, *34*, 185–188.
- (21) Liu, C.; Song, X.; Rao, X.; Xing, Y.; Wang, Z.; Zhao, J.; Qiu, J. *Dyes Pigm.* **2014**, *101*, 85–92.
- (22) Liu, C.; Song, X.; Wang, Z.; Qiu, J. *ChemPlusChem* **2014**, *79*, 1472–1481.
- (23) Wu, W.; Cheng, C.; Wu, W.; Guo, H.; Ji, S.; Song, P.; Han, K.; Zhao, J.; Zhang, X.; Wu, Y.; Du, G. *Eur. J. Inorg. Chem.* **2010**, *2010*, 4683–4696.
- (24) Wu, W.; Sun, J.; Ji, S.; Wu, W.; Zhao, J.; Guo, H. *Dalton Trans.* **2011**, *40*, 11550–11561.
- (25) Wu, W.; Wu, W.; Ji, S.; Guo, H.; Zhao, J. *Dalton Trans.* **2011**, *40*, 5953–5963.
- (26) Yang, X.; Peng, L.; Yuan, L.; Teng, P.; Tian, F.; Li, L.; Luo, S. *Opt. Commun.* **2011**, *284*, 3462–3466.
- (27) Ishiji, T.; Kaneko, M. *Analyst* **1995**, *120*, 1633–1638.
- (28) Schmärlzin, E.; van Dongen, J. T.; Klimant, I.; Marmodée, B.; Steup, M.; Fisahn, J.; Geigenberger, P.; Löhmannsröben, H.-G. *Biophys. J.* **2005**, *89*, 1339–1345.
- (29) Bizzarri, A.; Koehler, H.; Cajlakovic, M.; Pasic, A.; Schaupp, L.; Klimant, I.; Ribitsch, V. *Anal. Chim. Acta* **2006**, *573*, 48–56.
- (30) Amao, Y.; Miyashita, T.; Okura, I. *Analyst* **2000**, *125*, 871–875.
- (31) Amao, Y.; Asai, K.; Okura, I.; Shinohara, H.; Nishide, H. *Analyst* **2000**, *125*, 1911–1914.
- (32) Amao, Y.; Asai, K.; Miyashita, T.; Okura, I. *Polym. Adv. Technol.* **2000**, *11*, 705–709.
- (33) Amao, Y.; Miyashita, T.; Okura, I. *Anal. Chim. Acta* **2000**, *421*, 167–174.
- (34) Lee, S.; Kim, S.-O.; Shin, H.; Yun, H.-J.; Yang, K.; Kwon, S.-K.; Kim, J.-J.; Kim, Y.-H. *J. Am. Chem. Soc.* **2013**, *135*, 14321–14328.
- (35) Kozhevnikov, V. N.; Zheng, Y.; Clough, M.; Al-Attar, H. A.; Griffiths, G. C.; Abdullah, K.; Raisys, S.; Jankus, V.; Bryce, M. R.; Monkman, A. P. *Chem. Mater.* **2013**, *25*, 2352–2358.
- (36) Xing, Y.; Liu, C.; Song, X.; Li, J. *J. Mater. Chem. C* **2015**, *3*, 2166–2174.
- (37) Zhou, G.; Wang, Q.; Wong, W.-Y.; Ma, D.; Wang, L.; Lin, Z. *J. Mater. Chem.* **2009**, *19*, 1872–1883.
- (38) He, Z.; Wong, W.-Y.; Yu, X.; Kwok, H.-S.; Lin, Z. *Inorg. Chem.* **2006**, *45*, 10922–10937.
- (39) Brooks, J.; Babayan, Y.; Lamansky, S.; Djurovich, P. I.; Tsyba, I.; Bau, R.; Thompson, M. E. *Inorg. Chem.* **2002**, *41*, 3055–3066.
- (40) Zhou, G.; Wang, Q.; Wang, X.; Ho, C.-L.; Wong, W.-Y.; Ma, D.; Wang, L.; Lin, Z. *J. Mater. Chem.* **2010**, *20*, 7472–7484.
- (41) Demas, J.; DeGraff, B.; Xu, W. *Anal. Chem.* **1995**, *67*, 1377–1380.
- (42) Hartmann, P.; Leiner, M. J.; Kohlbacher, P. *Sens. Actuators, B* **1998**, *51*, 196–202.
- (43) Wai-SanLee, W.; ShingáChan, K. *J. Mater. Chem.* **1993**, *3*, 1031–1035.
- (44) Shriver, D. F.; Atkins, P. W.; Langford, C. H. *Inorganic Chemistry*, 2nd ed.; Oxford University: Oxford, 1990; pp 246–247.
- (45) Kataoka, Y.; Kitagawa, Y.; Kawakami, T.; Okumura, M. *J. Organomet. Chem.* **2013**, *743*, 163–169.
- (46) Roca-Lopez, D.; Polo, V.; Tejero, T.; Merino, P. *J. Org. Chem.* **2015**, *80*, 4076–4083.
- (47) Frisch, M. J.; Trucks, G. W.; Schlegel, H. B.; Scuseria, G. E.; Robb, M. A.; Cheeseman, J. R.; Scalmani, G.; Barone, V.; Mennucci, B.; Petersson, G. A.; Nakatsuji, H.; Caricato, M.; Li, X.; Hratchian, H. P.; Izmaylov, A. F.; Bloino, J.; Zheng, G.; Sonnenberg, J. L.; Hada, M.; Ehara, M.; Toyota, K.; Fukuda, R.; Hasegawa, J.; Ishida, M.; Nakajima, T.; Honda, Y.; Kitao, O.; Nakai, H.; Vreven, T.; Montgomery, J. A.; Peralta, J. E.; Ogliaro, F.; Bearpark, M.; Heyd, J. J.; Brothers, E.; Kudin, K. N.; Staroverov, V. N.; Kobayashi, R.; Normand, J.; Raghavachari, K.; Rendell, A.; Burant, J. C.; Iyengar, S. S.; Tomasi, J.; Cossi, M.; Rega, N.; Millam, J. M.; Klene, M.; Knox, J. E.; Cross, J. B.; Bakken, V.; Adamo, C.; Jaramillo, J.; Gomperts, R.; Stratmann, R. E.; Yazyev, O.; Austin, A. J.; Cammi, R.; Pomelli, C.; Ochterski, J. W.; Martin, R. L.; Morokuma, K.; Zakrzewski, V. G.; Voth, G. A.; Salvador, P.; Dannenberg, J. J.; Dapprich, S.; Daniels, A. D.; Farkas, O.; Foresman, J. B.; Ortiz, J. V.; Cioslowski, J.; Fox, D. J. *Gaussian, Revision A.02*; Gaussian, Inc.: Wallingford, CT, 2009.
- (48) Pavlishchuk, V. V.; Addison, A. W. *Inorg. Chim. Acta* **2000**, *298*, 97–102.